Tree-Sliced Variants of Wasserstein Distances

Tam Le[†]   Makoto Yamada[‡,†]   Kenji Fukumizu[◊,†]   Marco Cuturi[◁,▷]

RIKEN AIP[†], Kyoto University[‡]
The Institute of Statistical Mathematics, Japan[◊]
Google Brain, Paris[◁], CREST - ENSAE[▷]

October 29, 2019

Abstract

Optimal transport (OT) theory defines a powerful set of tools to compare probability distributions. OT suffers however from a few drawbacks, computational and statistical, which have encouraged the proposal of several regularized variants of OT in the recent literature, one of the most notable being the *sliced* formulation, which exploits the closed-form formula between univariate distributions by projecting high-dimensional measures onto random lines. We consider in this work a more general family of ground metrics, namely *tree metrics*, which also yield fast closed-form computations and negative definite, and of which the sliced-Wasserstein distance is a particular case (the tree is a chain). We propose the tree-sliced Wasserstein distance, computed by averaging the Wasserstein distance between these measures using random tree metrics, built adaptively in either low or high-dimensional spaces. Exploiting the negative definiteness of that distance, we also propose a positive definite kernel, and test it against other baselines on a few benchmark tasks.

1 Introduction

Many tasks in machine learning involve the comparison of two probability distributions, or histograms. Several geometries in the statistics and machine learning literature are used for that purpose, such as the Kullback-Leibler divergence, the Fisher information metric, the χ^2 distance, or the Hellinger distance, to name a few. Among them, the optimal transport (OT) geometry, also known as Wasserstein [65], Monge-Kantorovich [34], or Earth Mover's [54], has gained traction in the machine learning community [26, 39, 43], statistics [18, 50], or computer graphics [41, 61].

The naive computation of OT between two discrete measures involves solving a network flow problem whose computation scales typically cubically in the size of the measures [10]. There are two notable lines of work to reduce the time complexity of OT. *(i)* The first direction exploits the fact that simple ground costs can lead to faster computations. For instance, if one uses the binary metric $d(x,z) = \mathbb{1}_{x \neq z}$ between two points x, z, the OT distance is equivalent to the total variation distance [64, p.7]. When measures are supported on the real line $\mathbb{R}$ and the cost c is a nonegative convex function g applied to the difference $z - x$ between two points, namely for $x, z \in \mathbb{R}$, one has $c(x,z) = g(z - x)$, then the OT distance is equal to the integral of g evaluated on the difference between the generalized quantile functions of these two probability distributions [57, §2]. Other simplifications include thresholding the ground cost distance [51] or considering for a ground cost the shortest-path metric on a graph [52, §6]. *(ii)* The second one is to use regularization to approximate solutions of OT problems, notably entropy [14], which results in a problem that can be solved using Sinkhorn iterations. Genevay et al. [26] extended this approach to the semi-discrete

and continuous OT problems using stochastic optimization. Different variants of Sinkhorn algorithm have been proposed recently [4, 17], and speed-ups are obtained when the ground cost is the quadratic Euclidean distance [2, 3], or more generally the heat kernel on geometric domains [61]. The convergence of Sinkhorn algorithm has been considered in [4, 25].

In this work, we follow the first direction to provide a fast computation for OT. To do so, we consider tree metrics as ground costs for OT, which results in the so-called tree-Wasserstein (TW) distance [15, 21, 46]. We consider two practical procedures to sample tree metrics based on spatial information for both low-dimensional and high-dimensional spaces of supports. Using these random tree-metrics, we propose tree-sliced-Wasserstein distances, obtained by averaging over several TW distances with various ground tree metrics. The TW distance, as well as its average over several trees, can be shown to be negative definite[1]. As a consequence, we propose a positive definite tree-(sliced-)Wasserstein kernel that generalizes the sliced-Wasserstein kernel [11, 36].

The paper is organized as follows: we give reminders on OT and tree metrics in Section 2, introduce TW distance and its properties in Section 3, describe tree-sliced-Wasserstein variants with practical families of tree metrics, and proposed tree-(sliced)-Wasserstein kernel in Section 4, provide connections of TW with other work in Section 5, and follow with experimental results on many benchmark datasets in word embedding-based document classification and topological data analysis in Section 6, before concluding in Section 7. We have released code for these tools[2].

2 Reminders on Optimal Transport and Tree Metrics

In this section, we briefly review definitions of optimal transport (OT) and tree metrics. Let Ω be a measurable space endowed with a metric d. For any $x \in \Omega$, we write δ_x the Dirac unit mass on x.

Optimal transport. Let μ, ν be two Borel probability distributions on Ω, $\mathcal{R}(\mu, \nu)$ be the set of probability distributions π on the product space $\Omega \times \Omega$ such that $\pi(A \times \Omega) = \mu(A)$ and $\pi(\Omega \times B) = \nu(B)$ for all Borel sets A, B. The 1-Wasserstein distance W_d [64, p.2] between μ, ν is defined as:

$$W_d(\mu, \nu) = \inf \left\{ \int_{\Omega \times \Omega} d(x, z) \pi(dx, dz) \mid \pi \in \mathcal{R}(\mu, \nu) \right\}. \tag{1}$$

Let $\mathcal{F}_d$ be the set of Lipschitz functions w.r.t. d, i.e. functions $f : \Omega \to \mathbb{R}$ such that $|f(x) - f(z)| \leq d(x, z), \forall x, z \in \Omega$. The dual of (1) simplifies to the following problem OT [64, Theorem 1.3, p.19] is:

$$W_d(\mu, \nu) = \sup \left\{ \int_{\Omega} f(x) \mu(dx) - \int_{\Omega} f(z) \nu(dz) \mid f \in \mathcal{F}_d \right\}. \tag{2}$$

Tree metrics. A metric $d : \Omega \times \Omega \to \mathbf{R}$ is called a *tree metric* on Ω if there exists a tree $\mathcal{T}$ with non-negative edge lengths such that all elements of Ω are contained in its nodes and such that for every $x, z \in \Omega$, one has that $d(x, z)$ equals to the length of the (unique) path between x and z [58, §7, p.145–182]. We write the tree metric corresponding to that tree $d_{\mathcal{T}}$.

---

[1]In general, Wasserstein spaces are not Hilbertian [52, §8.3].
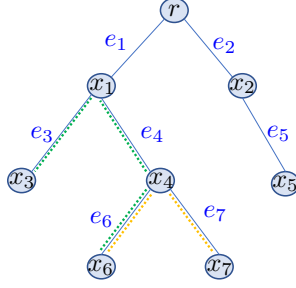[2]https://github.com/lttam/TreeWasserstein.

Figure 1: An illustration for a tree with root r where x_1, x_2 are at depth level 1, and x_6, x_7 are at depth level 3. Path $\mathcal{P}(x_3, x_6)$ contains e_3, e_4, e_6 (the green-dot path), $\Gamma(x_4) = \{x_4, x_6, x_7\}$ (the yellow-dot subtree), $v_{e_4} = x_4$, and $u_{e_4} = x_1$.

3 Tree-Wasserstein Distances: Optimal Transport with Tree Metrics

Lozupone and co-authors [44, 45] first noticed, when proposing the `UniFrac` method in the metagenomics community, that the Wasserstein distance between two measures supported on the nodes of the same tree admits a closed form when the ground metric between the supports of the two measures is a tree metric. That method was used to compare microbial communities by measuring the phylogenetic distance between sets of taxa in a phylogenetic tree as the fraction of the branch length of the tree that leads to descendants from either one environment or the other, but not both [44]. In this section, we follow [15, 21, 46] to leverage the geometric structure of tree metrics, and recall their main result.

Let $\mathcal{T}$ be a tree rooted at r with non-negative edge lengths, and $d_{\mathcal{T}}$ be the tree metric on $\mathcal{T}$. For nodes $x, z \in \mathcal{T}$, let $\mathcal{P}(x, z)$ be the (unique) path between x and z in $\mathcal{T}$, λ is the unique Borel measure (i.e. length measure) on $\mathcal{T}$ such that $d_{\mathcal{T}}(x, z) = \lambda(\mathcal{P}(x, z))$. We also write $\Gamma(x)$ for a set of nodes in the subtree of $\mathcal{T}$ rooted at x, defined as $\Gamma(x) = \{z \in \mathcal{T} \mid x \in \mathcal{P}(r, z)\}$. For each edge e in $\mathcal{T}$, let v_e be the deeper level node of edge e (farther to the root), u_e is the other node, and $w_e = d_{\mathcal{T}}(u_e, v_e)$ is the non-negative length of that edge, illustrated in Figure 1. Then, TW not only has a closed form, but is negative definite.

Proposition 1. *Given two measures μ, ν supported on $\mathcal{T}$, and setting the ground metric to be $d_{\mathcal{T}}$, then*

$$W_{d_{\mathcal{T}}}(\mu, \nu) = \sum_{e \in \mathcal{T}} w_e \left| \mu(\Gamma(v_e)) - \nu(\Gamma(v_e)) \right|. \tag{3}$$

Proof. Following [21], for any $f \in \mathcal{F}_{d_{\mathcal{T}}}$ such that $f(r) = 0$, there is an λ-a.e. unique Borel function $\mathtt{f} : \mathcal{T} \to [-1, 1]$ such that $f(x) = \int_{\mathcal{P}(r,x)} \mathtt{f}(z)\lambda(dz) = \int_{\mathcal{T}} \mathbb{1}_{z \in \mathcal{P}(r,x)} \mathtt{f}(z)\lambda(dz)$. Intuitively, $f(x)$ models a flow along the (unique) path of the root r and node x where $\mathtt{f}(z)$ controls a probability amount, received or provided by $f(x)$ on dz. Note that $\mathbb{1}_{z \in \mathcal{P}(r,x)} = \mathbb{1}_{x \in \Gamma(z)}$, then we have:

$$\int_{\mathcal{T}} f(x)\mu(dx) = \int_{\mathcal{T}} \int_{\mathcal{T}} \mathbb{1}_{z \in \mathcal{P}(r,x)} \mathtt{f}(z)\lambda(dz)\mu(dx) = \int_{\mathcal{T}} \mathtt{f}(z)\lambda(dz)\mu(\Gamma(z)).$$

Then, plugging this identity in Equation (2), we have:

$$W_{d_{\mathcal{T}}}(\mu, \nu) = \sup \left\{ \int_{\mathcal{T}} \left(\mu(\Gamma(z)) - \nu(\Gamma(z)) \right) \mathtt{f}(z)\lambda(dz) \right\} = \int_{\mathcal{T}} \left| \mu(\Gamma(z)) - \nu(\Gamma(z)) \right| \lambda(dz),$$

3

since the optimal function f^* corresponds to $\mathtt{f}(z) = 1$ if $\mu(\Gamma(z)) \geq \nu(\Gamma(z))$, otherwise $\mathtt{f}(z) = -1$. Moreover, we have $\mu(\Gamma(r)) = \nu(\Gamma(r)) = 1$, and $\lambda(\mathcal{P}(u_e, v_e)) = d_{\mathcal{T}}(u_e, v_e) = w_e$. Therefore,

$$W_{d_{\mathcal{T}}}(\mu, \nu) = \sum_{e \in \mathcal{T}} w_e \left| \mu(\Gamma(v_e)) - \nu(\Gamma(v_e)) \right|,$$

since the total mass flowing through edge e is equal to the total mass in subtree $\Gamma(v_e)$. $\square$

Proposition 2. *The tree-Wasserstein distance $W_{d_{\mathcal{T}}}$ is negative definite.*

Proof. Let m be the number of edges in tree $\mathcal{T}$. From Equation (3), $\mu(\Gamma(v_e))$ with $e \in \mathcal{T}$ can be considered as a feature map for probability distribution μ onto $\mathbb{R}_+^m$. Consequently, the TW distance is equivalent to a weighted ℓ_1 distance between these representations, with non-negative weights w_e, between these feature maps. Therefore, the tree-Wasserstein distance is negative definite[3]. $\square$

4 Tree-Sliced Wasserstein by Sampling Tree Metrics

Much as in sliced-Wasserstein (SW) distances, computing TW distances requires choosing or sampling tree metrics. Unlike SW distances however, the space of possible tree metrics is far too large in practical cases to expect that purely random trees can lead to meaningful results. We consider in this section two adaptive methods to define tree metrics based on spatial information in both low and high-dimensional cases, using partitioning or clustering. We further average the TW distances corresponding to these ground tree metrics. This has the benefit of reducing quantization effects, or cluster sensitivity problems in which data points may be partitioned or clustered to adjacent but different hypercubes [32] or clusters respectively. We then define the tree-sliced Wasserstein kernel, that is the direct generalization of those considered by [11, 36].

Definition 1. *For two measures μ, ν supported on a set in which tree metrics $\{ d_{\mathcal{T}_i} \mid 1 \leq i \leq n \}$ can be defined, the tree-sliced-Wasserstein (TSW) distance is defined as:*

$$\mathrm{TSW}(\mu, \nu) = \frac{1}{n} \sum_{i=1}^{n} W_{d_{\mathcal{T}_i}}(\mu, \nu). \tag{4}$$

Note that averaging of negative definite functions is trivially negative definite. Thus, following Definition 1 and Proposition 2, the TSW distance is also negative definite. Positive definite kernels can be therefore derived following [9, Theorem 3.2.2, p.74], and given $t > 0$, μ, ν on tree $\mathcal{T}$, we define the following tree-sliced-Wasserstein kernel,

$$k_{\mathrm{TSW}}(\mu, \nu) = \exp(-t\,\mathrm{TSW}(\mu, \nu)). \tag{5}$$

Very much like the Gaussian kernel, one can tune if needed the bandwidth parameter t according to the learning task that is targeted, using e.g. cross validation.

---

[3]We follow here [9, p. 66–67], to define negative-definiteness, see review about kernels in the appendix.

Adaptive methods to define tree metrics for the space of support data. We consider sampling mechanisms to select tree metrics to be used in Definition 1.

One possibility is to sample tree metrics following the general idea that these tree metrics should approximate the original distance [7, 8, 13, 22, 30]. This was the original motivation for previous work focusing on approximating the OT distance with the Euclidean ground metric (a.k.a. W_2 metric) into ℓ_1 metric for fast nearest neighbor search [16, 32]. Our goal is rather to sample tree metrics for the space of supports, and use those random tree metrics as ground metrics. Much like 1-dimensional projections do not offer interesting properties from a distortion perspective but remain useful for sliced-Wasserstein (SW) distance, we believe that trees with large distortions can be useful. This follows the recent realization that solving exactly the OT problem leads to overfitting [52, §8.4], and therefore excessive efforts to approximate the ground metric using trees would be self-defeating since it would lead to overfitting within the computation of the Wasserstein metric itself.

• **Partition-based tree metrics.** For low-dimensional spaces of supports, one can construct a partition-based tree metric with a tree structure $\mathcal{T}$ as follows:

Algorithm 1: `Partition_HC`$(\mathbf{s}, X, \tilde{x}_\mathbf{s}, \mathbf{h}, H_\mathcal{T})$

Input: $\mathbf{s}$: side-ℓ hypercube, X: set of m data points of $\mathbb{R}^\mathbf{d}$ in $\mathbf{s}$, $\tilde{x}_\mathbf{s}$: parent node, $\mathbf{h}$: a current depth level, and $H_\mathcal{T}$: the predefined deepest level of tree $\mathcal{T}$.

  1: **if** $m > 0$ **then**
  2:   **if** $\mathbf{h} > 0$ **then**
  3:     Node $\tilde{x}_c \leftarrow$ a point center of $\mathbf{s}$.
  4:     Length of edge $(\tilde{x}_\mathbf{s}, \tilde{x}_c) \leftarrow$ distance $(\tilde{x}_\mathbf{s}, \tilde{x}_c)$.
  5:   **else**
  6:     Node $\tilde{x}_c \leftarrow \tilde{x}_\mathbf{s}$.
  7:   **end if**
  8:   **if** $m > 1$ and $\mathbf{h} < H_\mathcal{T}$ **then**
  9:     Partition $\mathbf{s}$ into $2^\mathbf{d}$ side-$(\ell/2)$ hypercubes.
10:     **for each** side-$(\ell/2)$ hypercube $\mathbf{s}_c$ **do**
11:       $\tilde{X}_c \leftarrow$ data points of X in $\mathbf{s}_c$.
12:       `Partition_HC`$(\mathbf{s}_c, \tilde{X}_c, \tilde{x}_c, \mathbf{h}+1, H_\mathcal{T})$.
13:     **end for**
14:   **end if**
15: **end if**

Assume that data points are in a side-$(\beta/2)$ hypercube of $\mathbb{R}^\mathbf{d}$. We then randomly expand it into a hypercube $\mathbf{s}_0$ with side at most β. Inspired by a series of grids in [32], we set the center of $\mathbf{s}_0$ as the root of $\mathcal{T}$, and use a following recursive procedure to partition $\mathbf{s}_0$. For each side-ℓ hypercube $\mathbf{s}$, there are 3 partitioning cases: (i) if $\mathbf{s}$ does not contain any data points, we discard it, (ii) if $\mathbf{s}$ contains 1 data point, we use the center of $\mathbf{s}$ (or the data point) as a node in $\mathcal{T}$, and (iii) if $\mathbf{s}$ contains more than 1 data point, we represent $\mathbf{s}$ by its center as a node x in $\mathcal{T}$, and equally partition $\mathbf{s}$ into $2^\mathbf{d}$ side-$(\ell/2)$ hypercubes for potential child nodes of x. We then apply the recursive partition procedure for those child hypercubes. One can use any metrics in $\mathbb{R}^\mathbf{d}$ to obtain lengths for edges in $\mathcal{T}$. Additionally, one can use a predefined deepest level of $\mathcal{T}$ as a stopping condition for the procedure. We summarize the recursive tree construction procedure in Algorithm 1. As desired,

the random expansion of the original hypercube into $\mathbf{s}_0$ creates a variety to partition data spaces. Note that Algorithm 1 for constructing tree $\mathcal{T}$ is also known as the classical `Quadtree` algorithm [56] for 2-dimensional data (and later extended for high-dimensional data in [6, 30, 31, 32]).

• **Clustering-based tree metrics.** As in Algorithm 1, the number of partitioned hypercubes grows exponentially with respect to dimension $\mathbf{d}$. To overcome this problem for high-dimensional spaces, we directly leverage the distribution of support data points to adaptively partition data spaces via clustering, inspired by the clustering-based approach for a space subdivision in Improved Fast Gauss Transform [48, 66]. We derive a similar recursive procedure as in the partition-based tree metrics, but apply the farthest-point clustering [27] to partition support data points, and replace centers of hypercubes by cluster centroids as nodes in $\mathcal{T}$. In practice, we fix the same number of clusters κ when performing the farthest-point clustering (replace the partition in line 9 in Algorithm 1). κ is typically chosen via cross-validation. In general, one can apply any favorite clustering methods. We use the farthest-point clustering due to its fast computation. In particular, the complexity of the farthest-point clustering into κ clusters for n data points is $O(n \log \kappa)$ using the algorithm in [23]. Using different random initializations for the farthest-point clustering, we recover a simple sampling mechanism to obtain random tree metrics.

5   Relations to Other Work

OT with ground ultrametrics. An ultrametric is also known as non-Archimedean metric, or isosceles metric [59]. Ultrametrics strengthen the triangle inequality to a strong inequality (i.e., for any x, y, z in an ultrametric space, $d(x, z) \leq \max(d(x, y), d(y, z))$). Note that binary metrics are a special case of ultrametrics since binary metrics satisfy the strong inequality. Following [33, §1, p.245–247], an ultrametric implies a tree structure which can be constructed by hierarchical clustering schemes. Therefore, an ultrametric is a tree metric. Furthermore, we note that ultrametrics have similar spirits with strong kernels and hierarchy-induced kernels which are key components to form valid optimal assignment kernels for graph classification applications [37].

Connection with OT with Euclidean ground metric $W_2(\cdot, \cdot)$. Let $d_{\mathcal{T}}^H$ be a partition-based tree metric where H is the depth level of corresponding tree $\mathcal{T}$, at which all support data points are separated into different hypercubes (i.e., Algorithm 1 stops at depth level H). Edges in $\mathcal{T}$ are computed by Euclidean distance. Let β be the side of the randomly expanded hypercube. Given two $\mathbf{d}$-dimensional point clouds $\tilde{\mu}, \tilde{\nu}$ with the same cardinality (i.e., discrete uniform measures), and denote TW with $d_{\mathcal{T}}^H$ as $W_{d_{\mathcal{T}}^H}$. Then,

$$W_2(\tilde{\mu}, \tilde{\nu}) \leq W_{d_{\mathcal{T}}^H}(\tilde{\mu}, \tilde{\nu})/2 + \beta\sqrt{\mathbf{d}}/2^H.$$

The proof is given in the appendix material. Moreover, we also investigate the empirical relation between the TSW distance and the W_2 distance in the appendix material, in which empirical results indicate that the TSW distance agrees more with W_2 as the number of tree-slices used to define the TSW distance is increased.

Connection with embedding W_2 metric into ℓ_1 metric for fast nearest neighbor search. As discussed earlier, our goal is neither to approximate OT distance using trees as in [7, 8, 13, 22, 30],

nor to embed W_2 metric into ℓ_1 metric as in [16, 32], but rather to sample tree metrics to define an extended variant of the sliced-Wasserstein distance. When using the `Quadtree` algorithm (as in Algorithm 1) to sample tree metrics for the TSW distance, then the resulted TSW distance is in the same spirit as the embedding approach in [32] where the authors embedded W_2 metric into ℓ_1 metric by using a series of grids.

OT with tree metrics. There are a few work related to our considered class of OT with tree metrics [35, 62]. In particular, Kloeckner [35] studied geometric properties of OT space for measures on an ultrametric space, and Sommerfeld and Munk [62] focused on statistical inference for empirical OT on finite spaces including tree metrics.

6   Experimental Results

In this section, we evaluated the proposed TSW kernel k_{TSW} (Equation (5)) for comparing empirical measures in word embedding-based document classification and topological data analysis.

6.1   Word Embedding-based Document Classification

Kusner et al. [39] proposed Word Mover's distances for document classification. Each document is regarded as an empirical measure where each word and its frequency are considered as a support and a corresponding weight respectively. Kusner et al. [39] used word embedding such as *word2vec* to map each word to a vector data point. Equivalently, Word Mover's distances are OT metrics between empirical measures (i.e., documents) where its ground cost is a metric on the word embedding space.

Setup. We evaluated k_{TSW} on four datasets: `TWITTER`, `RECIPE`, `CLASSIC` and `AMAZON`, following the approach of Word Mover's distances [39], for document classification with SVM. Statistical characteristics for those datasets are summarized in Figure 2b. We used the *word2vec* word embedding [47], pre-trained on Google News[4], containing about 3 million words/phrases. *word2vec* maps these words/phrases into vectors in $\mathbb{R}^{300}$. Following [39], for all datasets, we removed all SMART stop word [55], and further dropped words in documents if they are not available in the pre-trained *word2vec*. We used two baseline kernels in the form of $\exp(-td)$ where d is a document distance and $t > 0$, for two corresponding baseline document distances based on Word Mover's: (i) OT with Euclidean ground metric [39], and (ii) sliced-Wasserstein, denoted as k_{OT} and k_{SW} respectively. For TSW distance in k_{TSW}, we consider n_s randomized clustering-based tree metrics, built with a predefined deepest level $H_{\mathcal{T}}$ of tree $\mathcal{T}$ as a stopping condition. We also regularized for kernel k_{OT} matrices due to its indefiniteness by adding a sufficiently large diagonal term as in [14]. For SVM, we randomly split each dataset into 70%/30% for training and test with 100 repeats, choose hyper-parameters through cross validation, choose $1/t$ from $\{1, q_{10}, q_{20}, q_{50}\}$ where q_s is the $s\%$ quantile of a subset of corresponding distances, observed on a training set, use one-vs-one strategy with Libsvm [12] for multi-class classification, and choose SVM regularization from $\{10^{-2:1:2}\}$. We ran experiments with Intel Xeon CPU E7-8891v3 (2.80GHz), and 256GB RAM.

---

[4]https://code.google.com/p/word2vec

6.2 Topological Data Analysis (TDA)

TDA has recently gained interest within the machine learning community [11, 38, 42, 53]. TDA is a powerful tool for statistical analysis on geometric structured data such as linked twist maps, or material data. TDA employs algebraic topology methods, such as persistence homology, to extract robust topological features (i.e., connected components, rings, cavities) and output 2-dimensional point multisets, known as persistence diagrams (PD) [19]. Each 2-dimensional point in PD summarizes a lifespan, corresponding to birth and death time as its coordinates, of a particular topological feature.

Setup. We evaluated k_{TSW} for orbit recognition and object shape classification with support vector machines (SVM), as well as change point detection for material data analysis with kernel Fisher discriminant ratio (KFDR) [28]. Generally, we followed the same setting as in [42] for these TDA experiments. We considered five baseline kernels for PD: (i) persistence scale space (k_{PSS}) [53], (ii) persistence weighted Gaussian (k_{PWG}) [38], (iii) sliced-Wasserstein (k_{SW}) [11], (iv) persistence Fisher (k_{PF}) [42], and (v) optimal transport[5], defined as $k_{\mathrm{OT}} = \exp(-td_{\mathrm{OT}})$ for $t > 0$, and also further regularized its kernel matrices by adding a sufficiently large diagonal term due to its indefiniteness as in §6.1. For TSW distance in k_{TSW}, we considered n_s randomized partition-based tree metrics, built with a predefined deepest level $H_{\mathcal{T}}$ of tree $\mathcal{T}$ as a stopping condition.

Let $\mathrm{Dg}_i = (x_1, x_2, \ldots, x_n)$ and $\mathrm{Dg}_j = (z_1, z_2, \ldots, z_m)$ be two PD where $x_i \mid_{1 \le i \le n}, z_j \mid_{1 \le j \le m} \in \mathbb{R}^2$, and $\Theta = \{(a, a) \mid a \in \mathbb{R}\}$ be the diagonal set. Denote $\mathrm{Dg}_{i\Theta} = \{\Pi_\Theta(x) \mid x \in \mathrm{Dg}_i\}$ where $\Pi_\Theta(x)$ is a projection of x on Θ. As in SW distance between Dg_i and Dg_j [11], we use transportation plans between $(\mathrm{Dg}_i \cup \mathrm{Dg}_{j\Theta})$ and $(\mathrm{Dg}_j \cup \mathrm{Dg}_{i\Theta})$ for TW (in Equation (4) of TSW) and OT distances. We typically used a cross validation to choose hyper-parameters, and followed corresponding authors of those baseline kernels to form sets of candidates. For k_{TSW} and k_{OT}, we chose $1/t$ from $\{1, q_{10}, q_{20}, q_{50}\}$. Similar as in §6.1, we used one-vs-one strategy with Libsvm for multi-class classification, $\{10^{-2:1:2}\}$ as a set of regularization candidates, and a random split 70%/30% for training and test with 100 repeats for SVM, and DIPHA toolbox[6] to extract PD.

Orbit recognition. Adams et al. [1, §6.4.1] proposed a synthesized dataset for link twist map, a discrete dynamical system to model flows in DNA microarrays [29]. There are 5 classes of orbits. As in [42], we generated 1000 orbits for each class where each orbit contains 1000 points. We considered 1-dimensional topological features for PD, extracted with Vietoris-Rips complex filtration [19].

Object shape classification. We evaluated object shape classification on a 10-class subset of MPEG7 dataset [40], containing 20 samples for each class as in [42]. For simplicity, we used the same procedure as in [42] to extract 1-dimensional topological features for PD with Vietoris-Rips complex filtration[7] [19].

Change point detection for material data analysis. We considered granular packing system [24] and SiO_2 [49] datasets for change point detection problem with KFDR as a statistical score.

---

[5]We used a fast OT implementation (e.g. on MPEG7 dataset, it took 7.98 seconds while the popular mex-file with Rubner's implementation required 28.72 seconds).

[6]https://github.com/DIPHA/dipha

[7]Turner et al. [63] proposed a more complicated and advanced filtration for this task.

As in [38, 42], we extracted 2-dimensional topological features for PD in granular packing system dataset, 1-dimensional topological features for PD in SiO_2 dataset, both with ball model filtration, and set 10^{-3} for the regularization parameter in KFDR. KFDR graphs for these datasets are shown in Figure 2c. For granular tracking system dataset, all kernel approaches obtain the change point as the 23rd index, which support an observation result (corresponding id = 23) in [5] . For SiO_2 dataset, results of all kernel methods are within a supported range ($35 \leq id \leq 50$), obtained by a traditional physical approach [20]. The KFDR results of k_{TSW} compare favorably with those of other baseline kernels. As shown in Figure 2b, k_{TSW} is faster than other baseline kernels. We note that we omit the baseline kernel k_{OT} for this application since computation of OT distance is out of memory.

6.3 Results of SVM, Time Consumption and Discussion

The results of SVM and time consumption for kernel matrices in TDA, and word embedding based document classification are illustrated in Figure 2a and Figure 2b respectively. The performances of k_{TSW} compare favorably with other baseline kernels. Moreover, the computational time of k_{TSW} is much less than that of k_{OT}. Especially, in CLASSIC dataset, it took less than 3 hours for k_{TSW} while more than 8 days for k_{OT}. Note that k_{TSW} and k_{SW} are positive definite while k_{OT} is not. The indefiniteness of k_{OT} may affect its performances in some applications, e.g. k_{OT} performs worse in TDA applications, but works well for documents with word embedding applications. The fact that SW only considers 1-dimensional projections may limit its ability to capture high-dimensional structure in data distributions [60]. TSW distance remedies this problem by using clustering-based tree metrics which directly leverage distributions of support data points. Furthermore, we also illustrate a trade-off of performances and computational time for different parameters in tree-sliced-Wasserstein distances for k_{TSW} on TWITTER dataset in Figure 3. For tree-sliced-Wasserstein TSW for k_{TSW}, performances are usually improved with more slices (n_s), but they come with a trade-off of more computational time. In these applications, we observed that a good trade-off for n_s of tree-sliced-Wasserstein is about 10 slices. Many further results can be seen in the appendix.

7 Conclusion

In this work, we proposed positive definite tree-(sliced)-Wasserstein kernel on OT geometry by considering a particular class of ground metrics, namely tree metrics. Much like the univariate Wasserstein distance, the tree-(sliced)-Wasserstein distance has a closed form, and is also negative definite. We also provide two sampling schemes to generate tree metrics for both high-dimensional and low-dimensional spaces. Leveraging random tree-metrics, we have proposed a new generalization of sliced-Wasserstein metrics that has more flexibility and degrees of freedom, by choosing a tree rather than a line, especially in high-dimensional spaces. The questions of sampling efficiently tree metrics from data points for tree-sliced-Wasserstein distance, as well as using them for more involved parametric inference are left for future work.
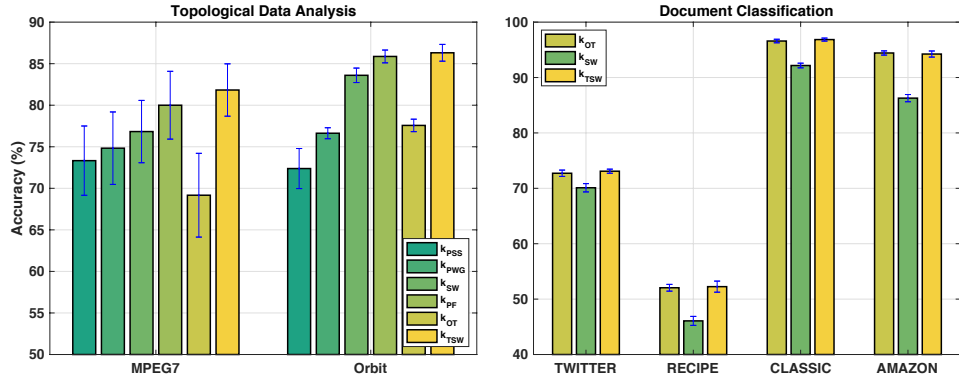
(a) SVM results for TDA and document classification.
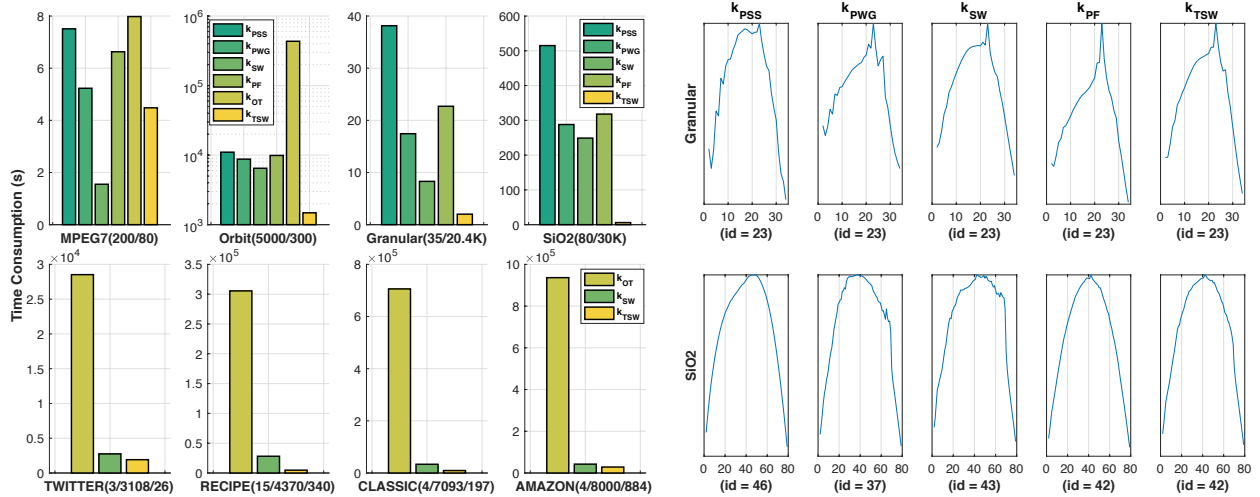
(b) Corresponding time consumption of kernel matrices for TDA and document classification.

(c) The KFDR graphs on granular packing system and SiO$_2$ datasets.

Figure 2: Experimental results. In (a), for a trade-off between time consumption and performances, results of TDA are reported for k_{TSW} with $(n_s = 6, H_{\mathcal{T}} = 6)$, and $(n_s = 12, H_{\mathcal{T}} = 5)$ in MPEG7 and Orbit datasets respectively. For document classification, results are reported for k_{SW} with $(n_s = 20)$, and for k_{TSW} with $(n_s = 10, H_{\mathcal{T}} = 6, \kappa = 4)$. In (b), the numbers in the parenthesis: for TDA (the first row), are the number of PD and the maximum number of points in PD respectively; for document classification (the second row), are the number of classes, the number of documents, and the maximum number of unique words for each document respectively. In (c), for k_{TSW}, TSW distances are computed with $(n_s = 12, H_{\mathcal{T}} = 6)$.
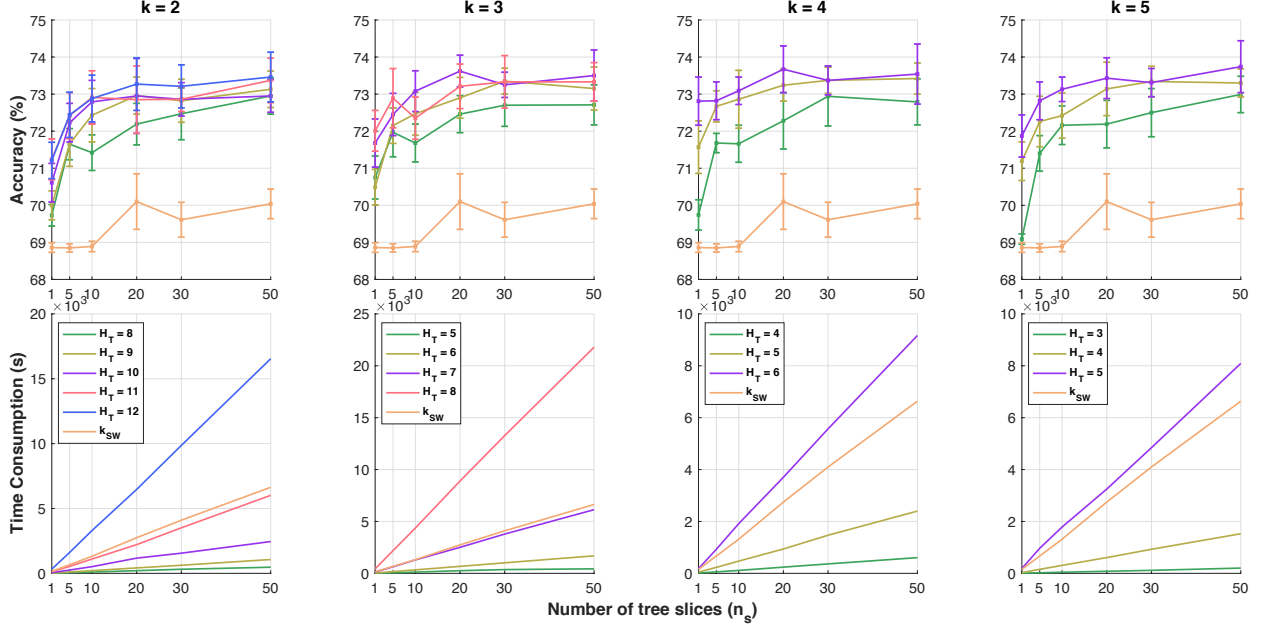
Figure 3: SVM results and time consumption of kernel matrices of k_{TSW} with different $(n_s, H_{\mathcal{T}}, \kappa)$, and k_{SW} with different n_s on `TWITTER` dataset.

A Detailed Proofs

In this section, we give detailed proofs for the inequality in the connection with OT with Euclidean ground metric (i.e. W_2 metric) for TW distance, and investigate an empirical relation between TSW and W_2 metric, especially when one increases the number of tree-slices in TSW. Additionally, we also provide proofs for negative definiteness of ℓ_1 distance (used in the proof of Proposition 2 in the main text), and indefinite divisibility for TSW kernel.

A.1 Proof of: $W_2(\tilde{\mu}, \tilde{\nu}) \leq W_{d_{\mathcal{T}}^H}(\tilde{\mu}, \tilde{\nu})/2 + \beta\sqrt{\mathtt{d}}/2^H$

For two point clouds $\tilde{\mu}, \tilde{\nu}$ containing n data points $x_i \mid_{1 \leq i \leq n}, z_j \mid_{1 \leq j \leq n}$ respectively, let c be a ground cost metric, and Σ_n be the set of all permutations of n elements, the OT can be reformulated as an optimal assignment problem as follow:

$$W_c(\tilde{\mu}, \tilde{\nu}) = \min_{\sigma \in \Sigma_n} \frac{1}{n} \sum_{i=1}^{n} c(x_i, z_{\sigma(i)}). \tag{6}$$

At a height level i in $\mathcal{T}$, the maximum Euclidean distance between any two data points in a same hypercube, denoted as Δ_i, we have

$$\Delta_i = \beta\sqrt{\mathtt{d}}/2^i.$$

Let $E_{i(i+1)}$ be a set of all edges between a height level i and a height level $(i+1)$ in $\mathcal{T}$. So, for any $e \in E_{i(i+1)}$, we have

$$w_e = \beta\sqrt{\mathtt{d}}/2^{i+1}.$$

11

Let q_i be the number of matched pairs at a height level i. Consequently, $(n - q_i)$ is the number of unmatched pairs at the height level i. Moreover, for the number of unmatched pairs at the height level i, observe that

$$n - q_i = \frac{1}{2} \sum_{e \in E_{(i-1)i}} |\tilde{\mu}(\Gamma(v_e)) - \tilde{\nu}(\Gamma(v_e))|. \tag{7}$$

In the right hand side of Equation (7), for all edges between the height level $(i - 1)$ and i of tree $\mathcal{T}$. Note that the total mass in subtree $\Gamma(v_e)$ is equal to the total mass flowing through edge e, we have $\mathcal{P}(r, x)\,|_{x \in \tilde{\mu}}$ and $\mathcal{P}(r, z)\,|_{z \in \tilde{\nu}}$ count the total number of visits on each edge in $E_{i(i+1)}$ for $\tilde{\mu}$ and $\tilde{\nu}$ respectively, and their absolute different number is twice to the number of unmatched pairs at the height level i, as described in Equation (7).

Therefore, the TW distance is as follow:

$$W_{d_{\mathcal{T}}^H}(\tilde{\mu}, \tilde{\nu}) = \frac{1}{n} \sum_{i=0}^{H-1} 2w_{\bar{e}_{i(i+1)}}(n - q_{i+1}) = \frac{1}{n} \sum_{i=0}^{H-1} \Delta_i (n - q_{i+1}), \tag{8}$$

where $\bar{e}_{i(i+1)}$ is an edge in $E_{i(i+1)}$, and note that $\Delta_i = 2w_{\bar{e}_{i(i+1)}}$.

Moreover, we have $(q_i - q_{i+1})$ is the number of pairs matched at a height level i, but unmatched at a height level $(i + 1)$. Additionally, note that $q_0 = n$, $q_H = 0$, and $\Delta_i = \Delta_{i-1}/2$, then we have

$$W_2(\tilde{\mu}, \tilde{\nu}) \leq \frac{1}{n} \sum_{i=0}^{H-1} \Delta_i (q_i - q_{i+1}) \tag{9}$$

$$= W_{d_{\mathcal{T}}^H}(\tilde{\mu}, \tilde{\nu}) - \frac{1}{n} \sum_{i=0}^{H-1} \Delta_i (n - q_i) \tag{10}$$

$$= W_{d_{\mathcal{T}}^H}(\tilde{\mu}, \tilde{\nu}) - \frac{1}{n} \sum_{i=1}^{H} \Delta_{i-1}(n - q_i)/2 + \Delta_H \tag{11}$$

$$= W_{d_{\mathcal{T}}^H}(\tilde{\mu}, \tilde{\nu})/2 + \beta\sqrt{\mathtt{d}}/2^H. \tag{12}$$

For the first equal, we added and subtracted n for the term in the parenthesis and note Equation (8) for $W_{d_{\mathcal{T}}^H}$. For the second equal, in the second term, for the element with $i = 0$, note that $(n - q_0) = 0$, we added and subtracted the element with $i = H$. For the third equal, we grouped the first two terms and note that $\Delta_H = \beta\sqrt{\mathtt{d}}/2^H$ for the third term.

Empirical relation between TSW and OT with Euclidean ground metric. The hypercube tree-sliced metric (i.e. partition-based tree metric) is our suggestion to build practical tree metrics for TSW when used on low-dimensional data spaces. We emphasize that we do not try to mimic the Euclidean OT (i.e. W_2) or the sliced-Wasserstein (SW), but rather propose a variant of OT distance. As stated in the main text, SW is a special case of TSW. From an empirical point of view, we have carried out the following experiment to investigate an empirical relation between TSW and W_2 distance:

For a query point q, let p be its nearest neighbor w.r.t. TSW. Figure 4 illustrates that p is very likely among the top 5 on MPEG7 dataset, and top 10 on Orbit dataset, near neighbors on the W_2 space. Results are averaged over 1000 runs of random split 90%/10% for training and test. When the number of tree-slices in TSW increases, the W_2 near-neighbor rank of p is improved. These empirical results suggest that TSW may agree with some aspects of W_2.
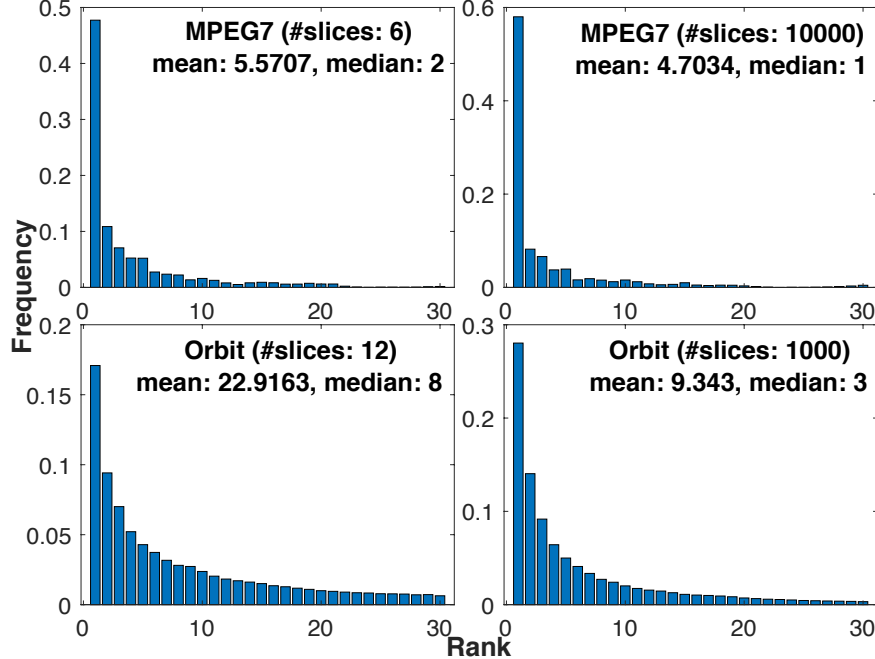
Figure 4: A frequency of near-neighbor rank on the W_2 space for the nearest neighbor w.r.t. TSW.

A.2 Proof of: Negative Definiteness for ℓ_1 Distance

For two real numbers a, b, the function $(a, b) \mapsto (a - b)^2$ is obviously negative definite. Following [9, Corollary 2.10, p.78], the function $(a, b) \mapsto |a - b|$ is negative definite. Therefore, ℓ_1 distance is a sum of negative definite functions. Thus, ℓ_1 distance is negative definite.

A.3 Indefinite Divisibility for Tree-Sliced-Wasserstein Kernel

Inspired by Le and Yamada [42], we derive the following proof of indefinite divisibility for the TSW kernel. For probability μ, ν on tree $\mathcal{T}$, and $i \in \mathbb{N}^*$, let $k_{\text{TSW}_i}(\mu, \nu) = \exp(-\frac{t}{i}\text{TSW}(\mu, \nu))$. We have $k_{\text{TSW}}(\cdot, \cdot) = (k_{\text{TSW}_i}(\cdot, \cdot))^i$, and $k_{\text{TSW}_i}(\cdot, \cdot)$ is positive definite. Following [9, §3, Definition 2.6, p.76], k_{TSW} is indefinitely divisible. Therefore, one does not need to recompute the Gram matrix of TSW kernel for each choice of t, since it indeed suffices to compute TSW distances between empirical measures in a training set once.

B More Experimental Results

We provide many further experimental results for our proposed tree-Wasserstein kernel on topological data analysis (TDA) and word embedding-based document classification.

B.1 Topological Data Analysis

Orbit recognition. Figure 5 shows SVM results and time consumption of kernel matrices of k_{TW} with different $(n_s, H_{\mathcal{T}})$ on Orbit dataset.
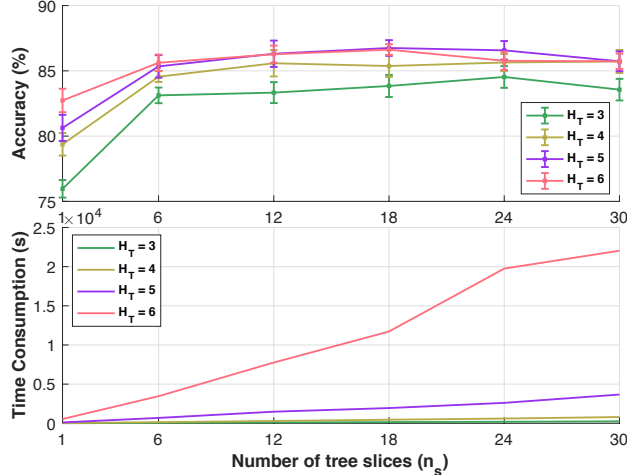
Figure 5: Results of SVM and time consumption of kernel matrices of k_{TW} with different $(n_s, H_{\mathcal{T}})$ on Orbit dataset.

Object shape classification. Figure 6 shows SVM results and time consumption of kernel matrices of k_{TW} with different $(n_s, H_{\mathcal{T}})$ on MPEG7 dataset.

Change point detection for material data analysis. Figure 7 and Figure 8 show time consumption of kernel matrices of k_{TW} with different $(n_s, H_{\mathcal{T}})$ on granular packing system and SiO_2 datasets respectively.

B.2 Word Embedding-based Document Classification

Figure 9, Figure 10, and Figure 11 show SVM results and time consumption of kernel matrices of k_{TW} with different $(n_s, H_{\mathcal{T}}, \kappa)$, and k_{SW} with different n_s on RECIPE, CLASSIC, and AMAZON datasets respectively.

C Brief Reviews of Kernels, the Farthest-Point Clustering, and the Synthesized Orbit Dataset

In this section, we give brief reviews for kernels, and the farthest-point clustering [27].Then, we provide details for the synthesized orbit dataset for orbit recognition).

C.1 A Brief Review of Kernels

We review some important definitions and theorems about kernels used in our work.

Positive definite kernels [9, p.66–67]. A kernel function $k : \mathcal{X} \times \mathcal{X} \to \mathbb{R}$ is positive definite if $\forall n \in \mathbb{N}^*, \forall x_1, x_2, ..., x_n \in \mathcal{X}, \sum_{i,j} c_i c_j k(x_i, x_j) \geq 0, \forall c_i \in \mathbb{R}$.

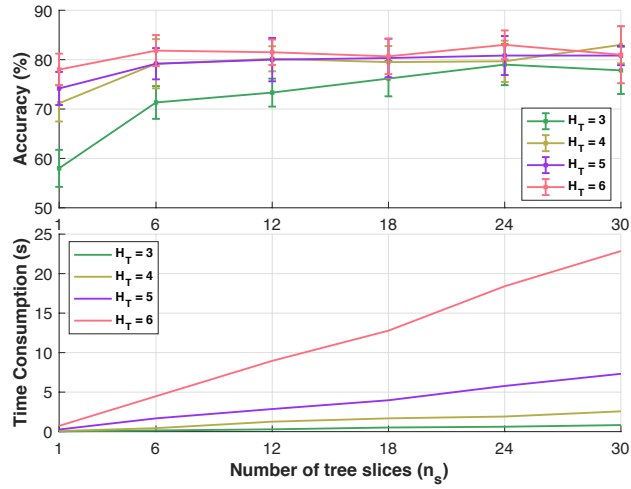Figure 6: Results of SVM and time consumption of kernel matrices of k_{TW} with different $(n_s, H_{\mathcal{T}})$ on MPEG7 dataset.
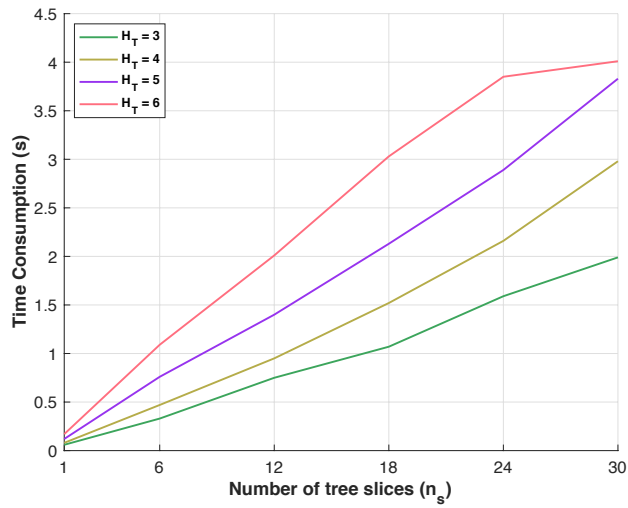

Figure 7: Time consumption of kernel matrices of k_{TW} with different $(n_s, H_{\mathcal{T}})$ on granular packing system dataset.
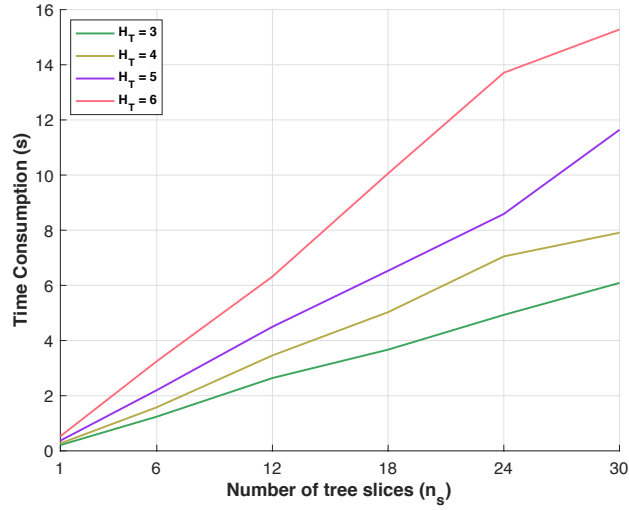
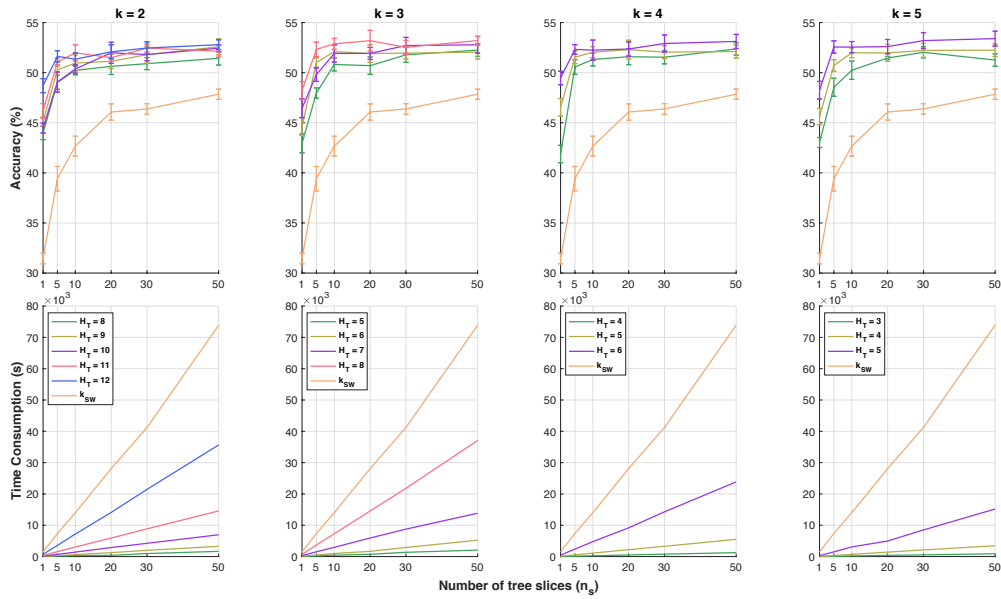Figure 8: Time consumption of kernel matrices of k_{TW} with different $(n_s, H_{\mathcal{T}})$ on SiO_2 dataset.

Figure 9: Results of SVM and time consumption of kernel matrices of k_{TW} with different $(n_s, H_{\mathcal{T}}, \kappa)$, and k_{SW} with different n_s on RECIPE dataset.
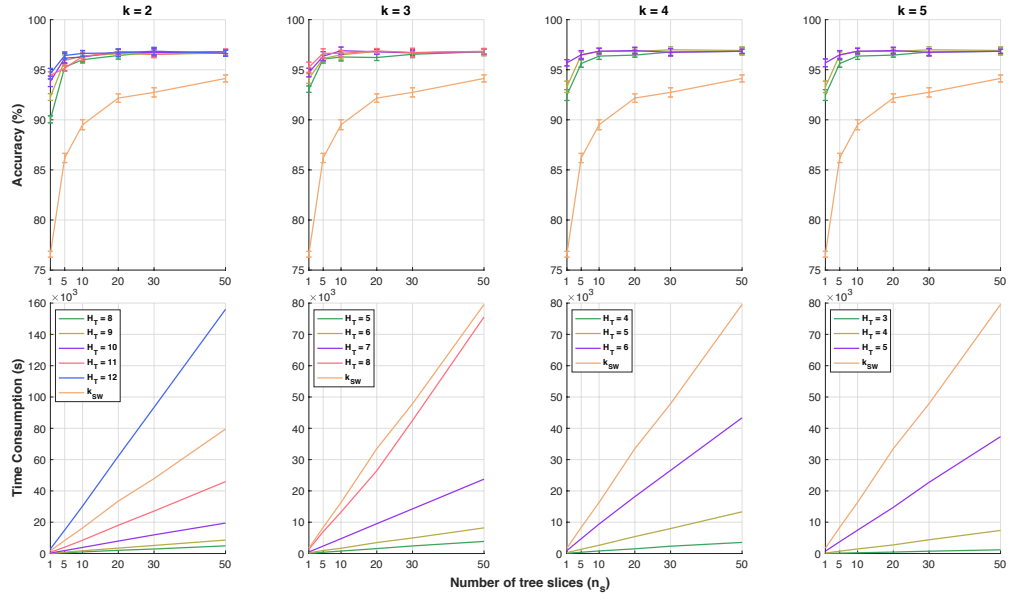
Figure 10: Results of SVM and time consumption of kernel matrices of k_{TW} with different $(n_s, H_{\mathcal{T}}, \kappa)$, and k_{SW} with different n_s on CLASSIC dataset.

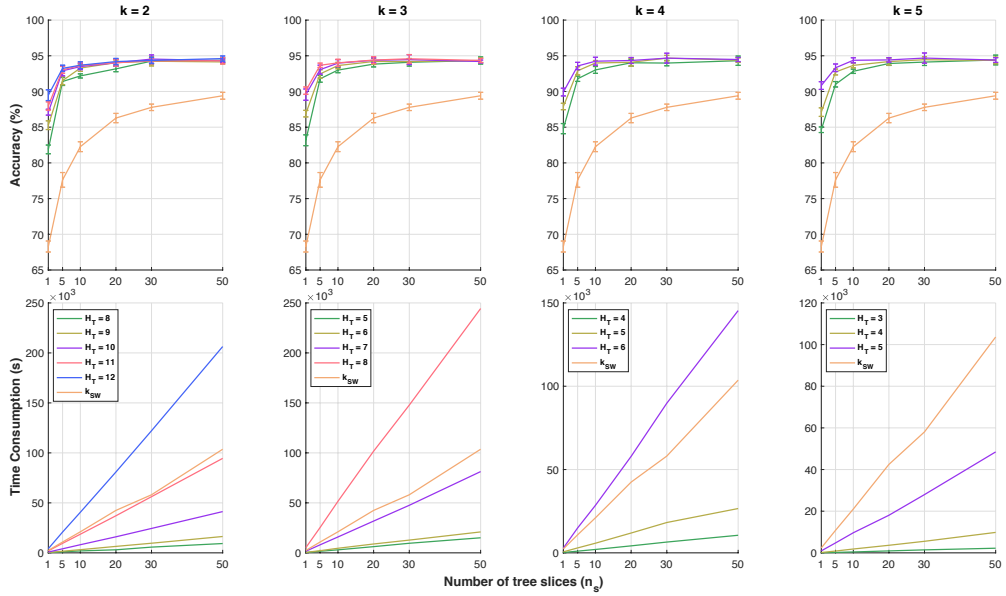
Figure 11: Results of SVM and time consumption of kernel matrices of k_{TW} with different $(n_s, H_{\mathcal{T}}, \kappa)$, and k_{SW} with different n_s on AMAZON dataset.

Negative definite kernels [9, p.66–67]. A kernel function $k : \mathcal{X} \times \mathcal{X} \to \mathbb{R}$ is negative definite if $\forall n \geq 2, \forall x_1, x_2, ..., x_n \in \mathcal{X}, \sum_{i,j} c_i c_j k(x_i, x_j) \leq 0, \forall c_i \in \mathbb{R}$ such that $\sum_i c_i = 0$.

Berg-Christensen-Ressel Theorem [9, Theorem 3.2.2, p.74]. If κ is a *negative definite* kernel, then kernel $k_t(x, z) := \exp\left(-t\kappa(x, z)\right)$ is positive definite for all $t > 0$.

C.2 A Brief Review of the Farthest-Point Clustering for Data Space Partition

The data space partition can be modeled as a κ-center problem. Given n data points $x_1, x_2, ..., x_n$, and a predefined number of clusters κ, the goal of κ-center problem is to find a partition of n points into κ clusters $\mathsf{S}_1, \mathsf{S}_2, ..., \mathsf{S}_\kappa$ as well as their corresponding centers $\mathsf{c}_1, \mathsf{c}_2, ..., \mathsf{c}_\kappa$ to minimize the maximum radius of clusters.

The farthest-point clustering [27] is a simple greedy algorithm, summarized in Algorithm 2. Gonzalez [27] also proved that the farthest-point clustering computes a partition with maximum radius at most twice the optimum for κ-center clustering. The complexity for a direct implementation for the farthest-point clustering as in Algorithm 2 is $O(n\kappa)$. This complexity can be reduced into $O(n \log \kappa)$ by using the algorithm in [23].

Algorithm 2: Farthest_Point_Clustering(X, κ)

Input: $X = (x_1, x_2, \ldots, x_n)$: a set of n data points, and κ: the predefined number of clusters.
Output: Clustering centers $\mathsf{c}_1, \mathsf{c}_2, ..., \mathsf{c}_\kappa$ and cluster index for each point x_i.
 1: $\mathsf{c}_1 \leftarrow$ a random point $x \in X$.
 2: Set of cluster $C \leftarrow \mathsf{c}_1$.
 3: $i \leftarrow 1$.
 4: **while** $i < \kappa$ and $n - i > 0$ **do**
 5: $\quad i \leftarrow i + 1$.
 6: $\quad \mathsf{c}_i \leftarrow \max_{x_j \in X} \min_{\mathsf{c} \in C} \|x_j - \mathsf{c}\|$. (a farthest point $x_j \in X$ to C).
 7: $\quad C \leftarrow C \cup \mathsf{c}_i$. (Add the new center into C).
 8: **end while**
 9: Each data point $x_j \in X$ is assigned to its nearest center $\mathsf{c}_i \in C$.

C.3 Details of the Synthesized Orbit Dataset

Adams et al. [1, §6.4.1] proposed a synthesized dataset for link twist map, a discrete dynamical system to model flows in DNA microarrays [29].

Given an initial position $(a_0, b_0) \in [0, 1]^2$, and $t > 0$, an orbit is modeled as

$$a_{i+1} = \quad a_i + t b_i(1 - b_i) \mod 1, \tag{13}$$

$$b_{i+1} = \quad b_i + t a_{i+1}(1 - a_{i+1}) \mod 1. \tag{14}$$

There are 5 classes, corresponding to 5 different parameters $t = 2.5, 3.5, 4, 4.1, 4.3$. For each class, we generated 1000 orbits with random initial positions where each orbit contains 1000 points.
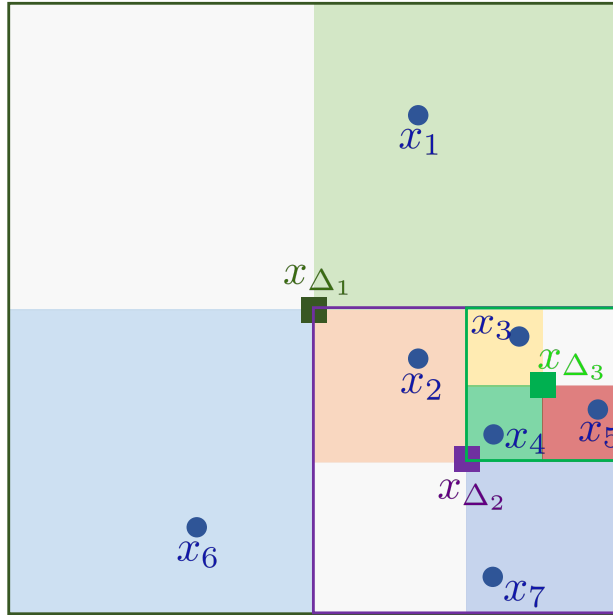
Figure 12: An example about the partition-based tree metric for a set of points in a 2-dimensional space.
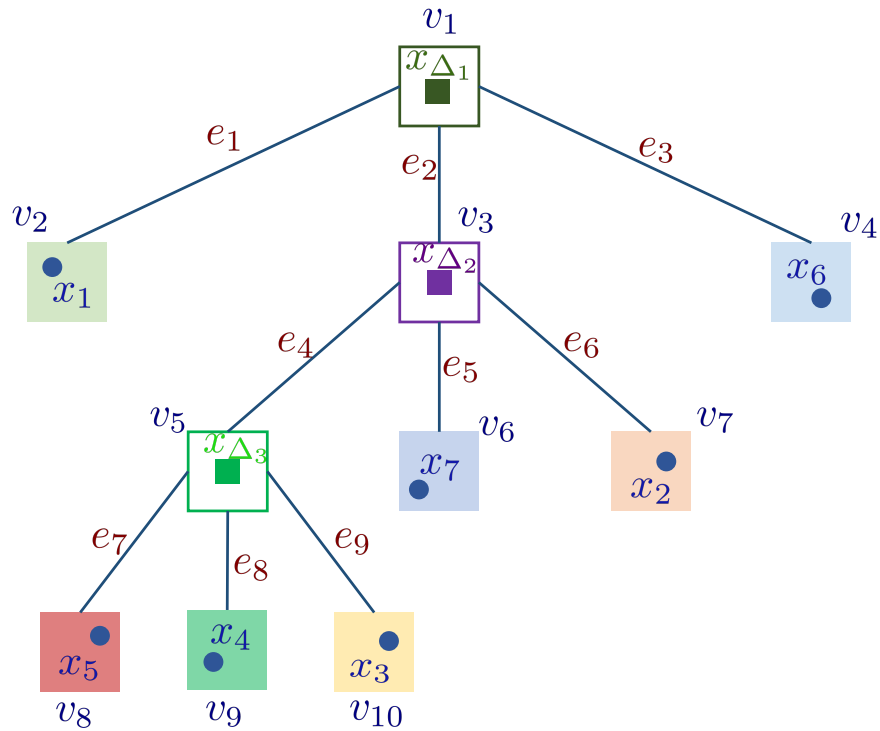

Figure 13: The corresponding tree structure for the example in Figure 12.

19

D   More Examples on the Partition-based Tree Metric, Quantization and Cluster Sensitivity Problems, and Persistence Diagrams

In this section, we give some examples for the partition-based tree metric, quantization and cluster sensitivity problems and persistence diagrams.

D.1   An Example on the Partition-based Tree Metric

Given a set X of 7 data points $x_i \mid_{1 \le i \le 7}$ in a 2-dimensional space as illustrated in Figure 12, one can choose a square region $\mathbf{s}_0$ as the largest square in Figure 12 containing all data points in X, and denote ℓ as the side of the largest square.

At height level 0 in tree $\mathcal{T}$, applying the `Partition_HC` algorithm for $\mathbf{s}_0$, one has x_{Δ_1} (center of $\mathbf{s}_0$) as a node (i.e., the root) represented for $\mathbf{s}_0$ in the constructed tree structure $\mathcal{T}$, and 4 child square regions[8] with side $\ell/2$, denoted $\mathbf{s}_{1a}$ (containing x_1), $\mathbf{s}_{1b}$ (containing x_2, x_3, x_4, x_5, x_7), $\mathbf{s}_{1c}$ (containing x_6), and $\mathbf{s}_{1d}$ (containing no data points). Therefore, one can discard $\mathbf{s}_{1d}$, use either data points (x_1, or x_6) or their centers represented for $\mathbf{s}_{1a}$ and $\mathbf{s}_{1c}$ respectively, and then apply the recursive procedure to partition for $\mathbf{s}_{1b}$ (at height level 1).

At height level 1 in tree $\mathcal{T}$, applying the `Partition_HC` algorithm for $\mathbf{s}_{1b}$, one has x_{Δ_2} (center of $\mathbf{s}_{1b}$) as a node represented for $\mathbf{s}_{1b}$ in the constructed tree structure $\mathcal{T}$, and 4 child square regions with side $\ell/4$, denoted $\mathbf{s}_{2a}$ (containing x_3, x_4, x_5), $\mathbf{s}_{2b}$ (containing x_7), $\mathbf{s}_{2c}$ (containing no data points), and $\mathbf{s}_{2d}$ (containing x_2). Therefore, one can discard $\mathbf{s}_{2c}$, use either data points (x_7, or x_2) or their centers represented for $\mathbf{s}_{2b}$ and $\mathbf{s}_{2d}$ respectively, and then apply the recursive procedure to partition for $\mathbf{s}_{2a}$ (at height level 2).

At height level 2 in tree $\mathcal{T}$, applying the `Partition_HC` algorithm for $\mathbf{s}_{2a}$, one has x_{Δ_3} (center of $\mathbf{s}_{2a}$) as a node represented for $\mathbf{s}_{2a}$ in the constructed tree structure $\mathcal{T}$, and 4 child square regions with side $\ell/8$, denoted $\mathbf{s}_{3a}$ (containing no data points), $\mathbf{s}_{3b}$ (containing x_5), $\mathbf{s}_{3c}$ (containing x_4), and $\mathbf{s}_{3d}$ (containing x_3). Therefore, one can discard $\mathbf{s}_{3a}$, and use either data points (x_5, or x_4, or x_3) or their centers represented for $\mathbf{s}_{3b}$, $\mathbf{s}_{3c}$ and $\mathbf{s}_{3d}$ respectively.

Hence, at the end, one obtains a tree structure $\mathcal{T}$ as illustrated in Figure 13, containing 10 nodes $v_i \mid_{1 \le i \le 10}$, and 9 edges $e_j \mid_{1 \le j \le 9}$. Node x_1 is the root of $\mathcal{T}$. The highest level in tree $\mathcal{T}$ is 3. For lengths of edges in $\mathcal{T}$, one can apply any metrics in the 2-dimensional space.

D.2   Some Examples and Discussion about the Quantization and Cluster Sensitivity Problems

The quantization or cluster sensitivity problem for partition or clustering is that some close data points are partitioned or clustered to adjacent, but different hypercubes or clusters respectively.

For example, in Figure 14, we illustrate different results of clustering, obtained with different initializations for the farthest-point clustering for a given 10000 random data points into 20 clusters. For data points near a border of adjacent, but different clusters, although they are very close to each other, they are still in different clusters, or known as a cluster sensitivity problem. Whether those data points are clustered into the same or different cluster(s), it depends on an initialization

---

[8]we use a clock order to enumerate for those child square regions: top right −¿ bottom right −¿ bottom left −¿ top left.
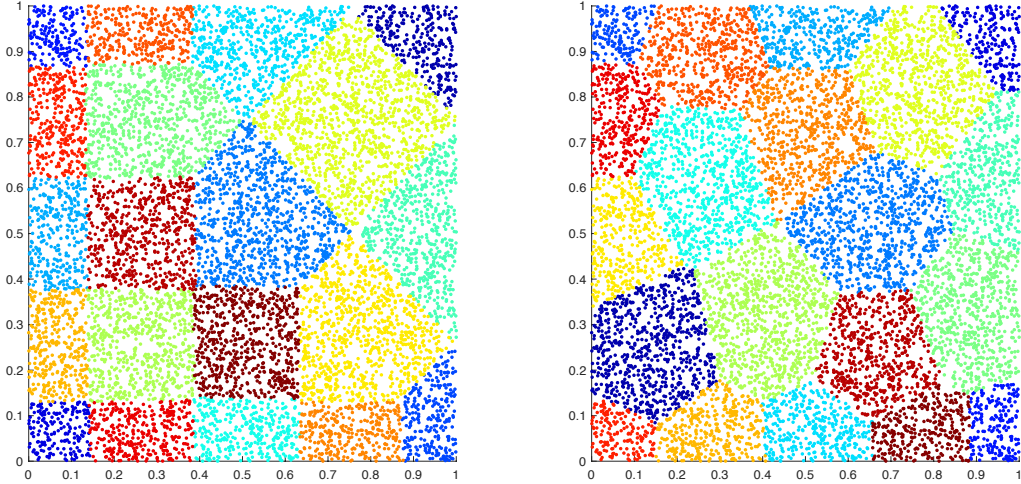
Figure 14: An illustration of the farthest-point clustering for 10000 data points into 20 clusters with different initializations.

of the farthest-point clustering. Therefore, by combining many different clustering results, obtained with various initializations for the farthest-point clustering algorithm, one can reduce an affect of the cluster sensitivity problem. Similarly for a quantization problem in the partition procedure (e.g. those data points near a border of adjacent, but different square regions of the same side in Figure 12).

D.3 An Example of Persistence Diagrams

In Figure 15, we give an example of a persistence diagram on a real-value function $f : \mathcal{X} \mapsto \mathbb{R}$. Persistence homology considers a family of sublevel sets $f^{-1}((-\infty, t])$. When t in $f^{-1}((-\infty, t])$ goes from $-\infty$ to $+\infty$, we collect all topological events, e.g., births and deaths of connected components (i.e., 0-dimensional topological features). As in Figure 15, connected components appears (i.e., birth) at $t = t_1, t_2$, and disappear (i.e., death) at $t = +\infty, t_3$ respectively. Therefore, persistence diagram of f is $\mathrm{Dg}f = \{(t_1, +\infty), (t_2, t_3)\}$.

References

[1] H. Adams, T. Emerson, M. Kirby, R. Neville, C. Peterson, P. Shipman, S. Chepushtanova, E. Hanson, F. Motta, and L. Ziegelmeier. Persistence images: A stable vector representation of persistent homology. *The Journal of Machine Learning Research*, 18(1):218–252, 2017. (Cited on pages 8 and 18.)

[2] J. Altschuler, F. Bach, A. Rudi, and J. Weed. Approximating the quadratic transportation metric in near-linear time. *arXiv preprint arXiv:1810.10046*, 2018. (Cited on page 2.)

[3] J. Altschuler, F. Bach, A. Rudi, and J. Weed. Massively scalable Sinkhorn distances via the Nystrom method. *arXiv preprint arXiv:1812.05189*, 2018. (Cited on page 2.)
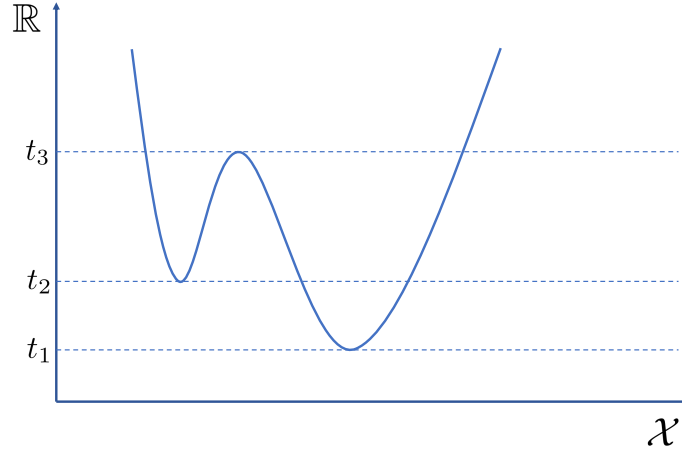
Figure 15: An example of a persistence diagram on a real-value function $f : \mathcal{X} \mapsto \mathbb{R}$. With sublevel sets $f^{-1}((-\infty, t])$ filtration, persistence diagram of f is $\mathrm{Dg}f = \{(t_1, +\infty), (t_2, t_3)\}$.

[4] J. Altschuler, J. Weed, and P. Rigollet. Near-linear time approximation algorithms for optimal transport via Sinkhorn iteration. In *Advances in Neural Information Processing Systems*, pages 1964–1974, 2017. (Cited on page 2.)

[5] Anonymous. What is random packing? *Nature*, 239:488–489, 1972. (Cited on page 9.)

[6] A. Backurs, P. Indyk, K. Onak, B. Schieber, A. Vakilian, and T. Wagner. Scalable fair clustering. In *International Conference on Machine Learning*, pages 405–413, 2019. (Cited on page 6.)

[7] Y. Bartal. Probabilistic approximation of metric spaces and its algorithmic applications. In *Proceedings of 37th Conference on Foundations of Computer Science*, pages 184–193, 1996. (Cited on pages 5 and 6.)

[8] Y. Bartal. On approximating arbitrary metrices by tree metrics. In *STOC*, volume 98, pages 161–168, 1998. (Cited on pages 5 and 6.)

[9] C. Berg, J. P. R. Christensen, and P. Ressel. *Harmonic analysis on semigroups*. Springer-Verlag, 1984. (Cited on pages 4, 13, 14, and 18.)

[10] R. E. Burkard and E. Cela. Linear assignment problems and extensions. In *Handbook of combinatorial optimization*, pages 75–149. Springer, 1999. (Cited on page 1.)

[11] M. Carriere, M. Cuturi, and S. Oudot. Sliced Wasserstein kernel for persistence diagrams. In *International Conference on Machine Learning*, volume 70, pages 664–673, 2017. (Cited on pages 2, 4, and 8.)

[12] C.-C. Chang and C.-J. Lin. Libsvm: a library for support vector machines. *ACM transactions on intelligent systems and technology (TIST)*, 2(3):27, 2011. (Cited on page 7.)

[13] M. Charikar, C. Chekuri, A. Goel, S. Guha, and S. Plotkin. Approximating a finite metric by a small number of tree metrics. In *Proceedings 39th Annual Symposium on Foundations of Computer Science*, pages 379–388, 1998. (Cited on pages 5 and 6.)

[14] M. Cuturi. Sinkhorn distances: Lightspeed computation of optimal transport. In *Advances in neural information processing systems*, pages 2292–2300, 2013. (Cited on pages 1 and 7.)

[15] K. Do Ba, H. L. Nguyen, H. N. Nguyen, and R. Rubinfeld. Sublinear time algorithms for Earth Mover's distance. *Theory of Computing Systems*, 48(2):428–442, 2011. (Cited on pages 2 and 3.)

[16] Y. Dong, P. Indyk, I. Razenshteyn, and T. Wagner. Scalable nearest neighbor search for optimal transport. *arXiv preprint arXiv:1910.04126*, 2019. (Cited on pages 5 and 6.)

[17] P. Dvurechensky, A. Gasnikov, and A. Kroshnin. Computational optimal transport: Complexity by accelerated gradient descent is better than by Sinkhorn's algorithm. In *Proceedings of the 35th International Conference on Machine Learning*, pages 1367–1376, 2018. (Cited on page 2.)

[18] J. Ebert, V. Spokoiny, and A. Suvorikova. Construction of non-asymptotic confidence sets in 2-Wasserstein space. *arXiv preprint arXiv:1703.03658*, 2017. (Cited on page 1.)

[19] H. Edelsbrunner and J. Harer. Persistent homology - a survey. *Contemporary mathematics*, 453:257–282, 2008. (Cited on page 8.)

[20] S. R. Elliott. Physics of amorphous materials. *Longman Group*, 1983. (Cited on page 9.)

[21] S. N. Evans and F. A. Matsen. The phylogenetic Kantorovich–Rubinstein metric for environmental sequence samples. *Journal of the Royal Statistical Society: Series B (Statistical Methodology)*, 74(3):569–592, 2012. (Cited on pages 2 and 3.)

[22] J. Fakcharoenphol, S. Rao, and K. Talwar. A tight bound on approximating arbitrary metrics by tree metrics. *Journal of Computer and System Sciences*, 69(3):485–497, 2004. (Cited on pages 5 and 6.)

[23] T. Feder and D. Greene. Optimal algorithms for approximate clustering. In *Proceedings of the twentieth annual ACM symposium on Theory of computing*, pages 434–444. ACM, 1988. (Cited on pages 6 and 18.)

[24] N. Francois, M. Saadatfar, R. Cruikshank, and A. Sheppard. Geometrical frustration in amorphous and partially crystallized packings of spheres. *Physical review letters*, 111(14):148001, 2013. (Cited on page 8.)

[25] J. Franklin and J. Lorenz. On the scaling of multidimensional matrices. *Linear Algebra and its applications*, 114:717–735, 1989. (Cited on page 2.)

[26] A. Genevay, M. Cuturi, G. Peyre, and F. Bach. Stochastic optimization for large-scale optimal transport. In *Advances in Neural Information Processing Systems*, pages 3440–3448, 2016. (Cited on page 1.)

[27] T. F. Gonzalez. Clustering to minimize the maximum intercluster distance. *Theoretical Computer Science*, 38:293–306, 1985. (Cited on pages 6, 14, and 18.)

[28] Z. Harchaoui, E. Moulines, and F. R. Bach. Kernel change-point analysis. In *Advances in neural information processing systems*, pages 609–616, 2009. (Cited on page 8.)

[29] J.-M. Hertzsch, R. Sturman, and S. Wiggins. Dna microarrays: design principles for maximizing ergodic, chaotic mixing. *Small*, 3(2):202–218, 2007. (Cited on pages 8 and 18.)

[30] P. Indyk. Algorithmic applications of low-distortion geometric embeddings. In *Proceedings 42nd IEEE Symposium on Foundations of Computer Science*, pages 10–33, 2001. (Cited on pages 5 and 6.)

[31] P. Indyk, I. Razenshteyn, and T. Wagner. Practical data-dependent metric compression with provable guarantees. In *Advances in Neural Information Processing Systems*, pages 2617–2626, 2017. (Cited on page 6.)

[32] P. Indyk and N. Thaper. Fast image retrieval via embeddings. *International Workshop on Statistical and Computational Theories of Vision*, 2003. (Cited on pages 4, 5, 6, and 7.)

[33] S. C. Johnson. Hierarchical clustering schemes. *Psychometrika*, 32(3):241–254, 1967. (Cited on page 6.)

[34] L. V. Kantorovich. On the transfer of masses. In *Dokl. Akad. Nauk. SSSR*, volume 37, pages 227–229, 1942. (Cited on page 1.)

[35] B. R. Kloeckner. A geometric study of Wasserstein spaces: ultrametrics. *Mathematika*, 61(1):162–178, 2015. (Cited on page 7.)

[36] S. Kolouri, Y. Zou, and G. K. Rohde. Sliced Wasserstein kernels for probability distributions. In *Proceedings of the IEEE Conference on Computer Vision and Pattern Recognition (CVPR)*, pages 5258–5267, 2016. (Cited on pages 2 and 4.)

[37] N. M. Kriege, P.-L. Giscard, and R. Wilson. On valid optimal assignment kernels and applications to graph classification. In *Advances in Neural Information Processing Systems*, pages 1623–1631, 2016. (Cited on page 6.)

[38] G. Kusano, K. Fukumizu, and Y. Hiraoka. Kernel method for persistence diagrams via kernel embedding and weight factor. *Journal of Machine Learning Research*, 18(189):1–41, 2018. (Cited on pages 8 and 9.)

[39] M. Kusner, Y. Sun, N. Kolkin, and K. Weinberger. From word embeddings to document distances. In *International Conference on Machine Learning*, pages 957–966, 2015. (Cited on pages 1 and 7.)

[40] L. J. Latecki, R. Lakamper, and T. Eckhardt. Shape descriptors for non-rigid shapes with a single closed contour. In *Proceedings of the IEEE Conference on Computer Vision and Pattern Recognition (CVPR)*, volume 1, pages 424–429, 2000. (Cited on page 8.)

[41] H. Lavenant, S. Claici, E. Chien, and J. Solomon. Dynamical optimal transport on discrete surfaces. In *SIGGRAPH Asia 2018 Technical Papers*, page 250. ACM, 2018. (Cited on page 1.)

[42] T. Le and M. Yamada. Persistence Fisher kernel: A Riemannian manifold kernel for persistence diagrams. In *Advances in Neural Information Processing Systems*, pages 10028–10039, 2018. (Cited on pages 8, 9, and 13.)

[43] J. Lee and M. Raginsky. Minimax statistical learning with Wasserstein distances. In *Advances in Neural Information Processing Systems*, pages 2692–2701, 2018. (Cited on page 1.)

[44] C. Lozupone and R. Knight. Unifrac: a new phylogenetic method for comparing microbial communities. *Applied and environmental microbiology*, 71(12):8228–8235, 2005. (Cited on page 3.)

[45] C. A. Lozupone, M. Hamady, S. T. Kelley, and R. Knight. Quantitative and qualitative β diversity measures lead to different insights into factors that structure microbial communities. *Applied and environmental microbiology*, 73(5):1576–1585, 2007. (Cited on page 3.)

[46] A. McGregor and D. Stubbs. Sketching Earth-Mover distance on graph metrics. In *Approximation, Randomization, and Combinatorial Optimization. Algorithms and Techniques*, pages 274–286. Springer, 2013. (Cited on pages 2 and 3.)

[47] T. Mikolov, I. Sutskever, K. Chen, G. S. Corrado, and J. Dean. Distributed representations of words and phrases and their compositionality. In *Advances in neural information processing systems*, pages 3111–3119, 2013. (Cited on page 7.)

[48] V. I. Morariu, B. V. Srinivasan, V. C. Raykar, R. Duraiswami, and L. S. Davis. Automatic online tuning for fast gaussian summation. In *Advances in neural information processing systems*, pages 1113–1120, 2009. (Cited on page 6.)

[49] T. Nakamura, Y. Hiraoka, A. Hirata, E. G. Escolar, and Y. Nishiura. Persistent homology and many-body atomic structure for medium-range order in the glass. *Nanotechnology*, 26(30):304001, 2015. (Cited on page 8.)

[50] V. M. Panaretos, Y. Zemel, et al. Amplitude and phase variation of point processes. *The Annals of Statistics*, 44(2):771–812, 2016. (Cited on page 1.)

[51] O. Pele and M. Werman. Fast and robust Earth Mover's distances. In *International Conference on Computer Vision*, pages 460–467, 2009. (Cited on page 1.)

[52] G. Peyré and M. Cuturi. Computational optimal transport. *Foundations and Trends in Machine Learning*, 11(5-6):355–607, 2019. (Cited on pages 1, 2, and 5.)

[53] J. Reininghaus, S. Huber, U. Bauer, and R. Kwitt. A stable multi-scale kernel for topological machine learning. In *Proceedings of the IEEE conference on computer vision and pattern recognition (CVPR)*, pages 4741–4748, 2015. (Cited on page 8.)

[54] Y. Rubner, C. Tomasi, and L. J. Guibas. The Earth Mover's distance as a metric for image retrieval. *International journal of computer vision*, 40(2):99–121, 2000. (Cited on page 1.)

[55] G. Salton and C. Buckley. Term-weighting approaches in automatic text retrieval. *Information processing & management*, 24(5):513–523, 1988. (Cited on page 7.)

[56] H. Samet. The quadtree and related hierarchical data structures. *ACM Computing Surveys (CSUR)*, 16(2):187–260, 1984. (Cited on page 6.)

[57] F. Santambrogio. *Optimal transport for applied mathematicians*. Birkhauser, 2015. (Cited on page 1.)

[58] C. Semple and M. Steel. Phylogenetics. *Oxford Lecture Series in Mathematics and its Applications*, 2003. (Cited on page 2.)

[59] S. A. Shkarin. Isometric embedding of finite ultrametric spaces in banach spaces. *Topology and its Applications*, 142(1-3):13–17, 2004. (Cited on page 6.)

[60] U. Şimşekli, A. Liutkus, S. Majewski, and A. Durmus. Sliced-Wasserstein flows: Nonparametric generative modeling via optimal transport and diffusions. *arXiv preprint arXiv:1806.08141*, 2018. (Cited on page 9.)

[61] J. Solomon, F. De Goes, G. Peyre, M. Cuturi, A. Butscher, A. Nguyen, T. Du, and L. Guibas. Convolutional wasserstein distances: Efficient optimal transportation on geometric domains. *ACM Transactions on Graphics (TOG)*, 34(4):66, 2015. (Cited on pages 1 and 2.)

[62] M. Sommerfeld and A. Munk. Inference for empirical Wasserstein distances on finite spaces. *Journal of the Royal Statistical Society: Series B (Statistical Methodology)*, 80(1):219–238, 2018. (Cited on page 7.)

[63] K. Turner, S. Mukherjee, and D. M. Boyer. Persistent homology transform for modeling shapes and surfaces. *Information and Inference: A Journal of the IMA*, 3(4):310–344, 2014. (Cited on page 8.)

[64] C. Villani. *Topics in optimal transportation*. American Mathematical Soc., 2003. (Cited on pages 1 and 2.)

[65] C. Villani. *Optimal transport: old and new*, volume 338. Springer Science and Business Media, 2008. (Cited on page 1.)

[66] C. Yang, R. Duraiswami, and L. S. Davis. Efficient kernel machines using the improved fast gauss transform. In *Advances in neural information processing systems*, pages 1561–1568, 2005. (Cited on page 6.)